# Supporting Information

Petroff and Libchaber 10.1073/pnas.1322092111

## SI Text

### Picture of a *Thiovulum majus* Veil

Fig. S1 shows a picture of a *Thiovulum majus* veil taken at the field site in the Little Sippewissett Salt Marsh in Falmouth, MA at low tide. This is the same veil shown in Fig. 1*C* of the main text. To find this veil, we walked through the salt marsh at low tide. Veils tend to form in shallow pools ($\sim 1-5$ cm deep) or at the bases of grass. The veils are most common in regions of the marsh where the smell of sulfide is intense.

### Estimates of Cell Parameters from Front Dynamics

In this section, we derive the scalings that relate the dynamics of a front of cells to the biological parameters. These results are used in *Formation of a Front* in the main text. The front moves up the oxygen gradient as cells from the front diffuse. Balancing the diffusive flux of cells with the front velocity, we find

$$U_f n_f \sim D_n \frac{n_f}{\sigma}. \quad [S1]$$

Similarly, the total flux of cells from the front into the tail must balance the reproduction of cells in the front. Balancing the chemotactic and diffusive fluxes with reproduction, we find

$$-D_n \frac{n_f - n_0}{\sigma} + \chi'(c^*)c^* \; n_0 \frac{c^*}{\sigma} \sim R_0 n_f c^* \sigma. \quad [S2]$$

We now impose conservation of oxygen and cell number. In steady state, the total flux of oxygen into the front $U_f c_\infty$ must balance the rate at which oxygen is consumed by cells. Thus,

$$U_f c_\infty \sim B_0 n_f c^* \sigma. \quad [S3]$$

Finally, the rate a which cells flow into the tail must match the rate at which cells are produced in the front. This constraint requires

$$U_f n_0 \sim R_0 n_f c^* \sigma. \quad [S4]$$

Using these scaling relations with estimates of $\sigma$, $U_f$, $n_f$, and $R_0$ (values provided in the main text), we solve for the metabolic rate $B_0$, density of cells in the tail $n_0$, the diffusion coefficient $D_n$, and the chemotaxis coefficient $\chi'(c^*)$. Of these, the first two are used in the main text.

The cell diffusion coefficient $D_n \sim 10^{-6}$ cm$^2$·s$^{-1}$ is an order of magnitude smaller than a typical value (1). The relatively small diffusion coefficient is consistent with the observations of Thar and Kühl, who argue that *T. majus* cells are large enough to directly measure chemical gradients (2).

The chemotaxis coefficient $\chi'(c^*) \sim 0.25$ cm$^2$·s$^{-1}$. Given a typical gradient of size $\ell = D_c/U_f = 0.1$ cm, this value of $\chi'(c^*)$ gives a typical swimming speed $U_s \sim c^*\chi'(c^*)/\lambda \sim 0.1$ cm·s$^{-1}$, which is within a factor of 2 of the observed swimming speed 0.06 cm·s$^{-1}$.

### Flow in a Hele-Shaw Chamber

In this section, we find the flow of water around a point force in a Hele-Shaw chamber. In a Hele-Shaw chamber, water flows down harmonic pressure gradients. A schematic of this system is shown in Fig. S3. We nondimensionalize the pressure field with the typical pressure $p_0 = f_0/b^2$, where $b$ is the thickness of the fluid layer. We approximate the influence of a cell attached to the veil with the lowest-order divergence-free singularity. We therefore must solve

$$\nabla^2 p = \hat{m} \cdot \nabla \delta(x)\delta(z), \quad [S5]$$

where $\hat{m}$ is the orientation of the cell in the Hele-Shaw chamber. Because water cannot flow through the impenetrable walls, we require that the normal component of the pressure gradient vanishes on the boundaries.

We solve this boundary-value problem by developing an image system. In the absence of the boundaries, the pressure field $p_\infty$ is given by

$$p_\infty = \frac{1}{2}\hat{m} \cdot \nabla \log\left(u^2 + v^2\right). \quad [S6]$$

To impose a single impenetrable boundary, as shown in Fig. S3, we simply reflect a single point force about the boundary. The resulting pressure field

$$p_b = \frac{1}{2}\hat{m} \cdot \nabla \log\left((u-u_0)^2 + (v-v_0)^2\right) + \frac{1}{2}\left(\hat{m} - 2\hat{m}\cdot\hat{v}\hat{v}\right) \cdot \nabla \log\left((u-u_0)^2 + (v+v_0)^2\right). \quad [S7]$$

Because the pressure field is harmonic, this solution can be used to construct new solutions through the use of conformal mappings. In particular, the complex function $x + iz = \zeta(u+iv) = i\log(u+iv)/\pi$ maps the real axis to the lines $x = 0$ and $x = -1$. Conformal mappings stretch and rotate vectors. The mapping increases the magnitude of the point force by a factor $|\zeta'|^2$ and rotates it an angle $\arg(u+iv)$. Correcting for these factors gives the pressure field around a unit point force with orientation $-\hat{z}$ centered at $(x_0, 0)$ between two parallel boundaries,

$$p_{hs} = p(x - x_0, z) + p(x + x_0, z), \quad [S8]$$

where

$$p = \frac{1 - e^{z/\pi w}\cos(x/\pi w)}{1 - 2e^{z/\pi w}\cos(x/\pi w) + e^{2z/\pi w}}. \quad [S9]$$

Notably, because $p$ is an even function of $x$, the total pressure field $p_{hs}$ can be divided into two parts. $p(x - x_0, z)$ creates a symmetric flow about the point force. The asymmetry of the flow results from the influence of the image point force $p(x + x_0, z)$.

### Cell Density Fluctuations

In this section, we find the rate at which a bacterial front of area $A$ and mean density $n_f$ generates density fluctuations of size $\delta n/\delta A$ over an area $\delta A$. Cells move as Brownian particles with diffusion coefficient $D_{eff}$.

From the central limit theorem, the number of cells $N$ within an area $\delta A$ is normally distributed with mean

$$\mu = \langle N \rangle = n_f \delta A \quad [S10]$$

and variance

$$\sigma^2 = \left\langle \left(N - \langle N \rangle\right)^2 \right\rangle = n_f \delta A. \quad [S11]$$

Thus, the probability of observing a density fluctuation larger than $\delta n/\delta A$ is

$$P = \int_{\delta n}^{\infty} \frac{e^{-x^2/(2n_f\delta A)}}{\sqrt{2\pi n_f \delta A}} \mathrm{d}x. \quad \textbf{[S12]}$$

The correlation time for density fluctuations of this size is $\tau = \delta A/D_{eff}$. Thus, the mean number of times $v$ one observes density fluctuations somewhere in the front of size $A$ after a time $t$ is

$$\nu = \frac{A}{\delta A}\frac{t}{\tau}P. \quad \textbf{[S13]}$$

Thus, the typical rate $k$ at which these fluctuations form is

$$k(\delta n, \delta A) = \frac{AD_{eff}}{\delta A^2} \int_{\delta n}^{\infty} \frac{e^{-x^2/(2n_f\delta A)}}{\sqrt{2\pi n_f \delta A}} \mathrm{d}x. \quad \textbf{[S14]}$$


1. Berg HC (1993) *Random Walks in Biology* (Princeton Univ Press, Princeton).

2. Thar R, Kühl M (2003) Bacteria are not too small for spatial sensing of chemical gradients: An experimental evidence. *Proc Natl Acad Sci USA* 100(10):5748–5753.


**Fig. S1.** A view of a naturally occurring *T. majus* veil from Little Sippewissett Salt Marsh in Falmouth, MA. (Scale bar, 1 cm.)

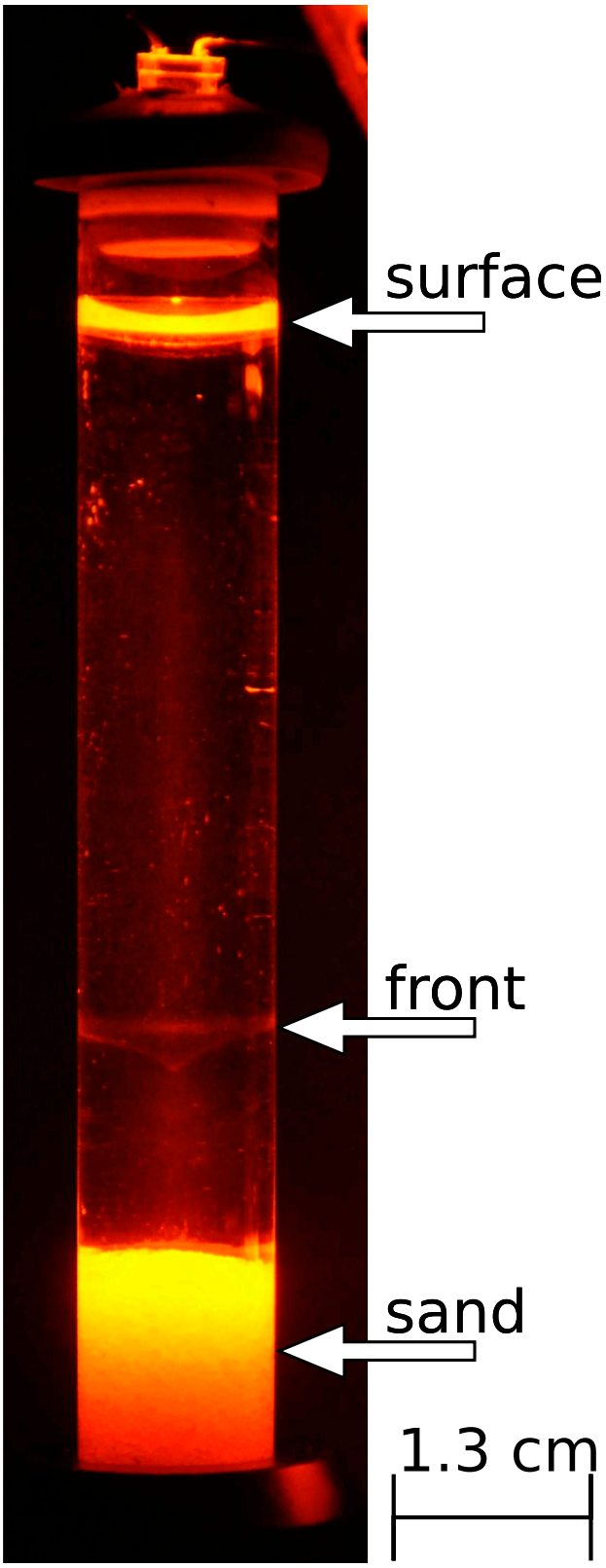


**Fig. S2.** A photograph of a *T. majus* front propagating up an oxygen gradient in a test tube.

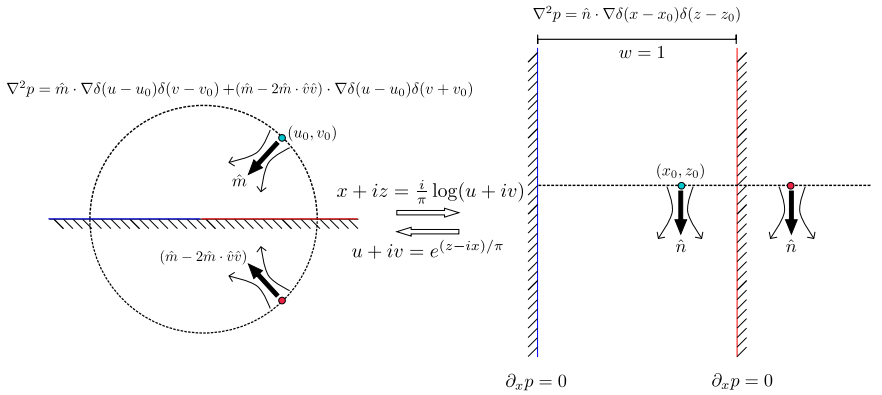


**Fig. S3.** To find the pressure field in a Hele-Shaw chamber, we develop an image system. We first find the pressure field due to a point force (blue dot) next to a single impenetrable boundary. We do so by placing an equal and opposite point force (red dot) on the other side of the boundary. Because the pressure field is harmonic, we can use this solution to construct new solutions using conformal mappings. In this case, we use a logarithmic mapping to find the pressure field due to a point force between two parallel walls. This mapping stretches and rotates the point force.

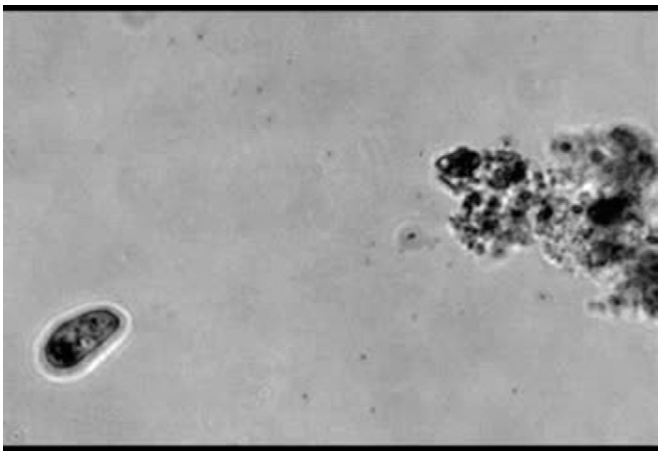

**Movie S1.** Single_cell.avi (Fig. 1*A* of the main text). A single *T. majus* cell from an environmental sample swims in place. As the cell beats its flagella while tethered to a piece of detritus, micron-scale particles are pulled past the cell. The length of the cell is ~20 μm. The motion of the mucus stalk connecting the cell to the detritus can be seen from the motion of several particles that have become stuck to the stalk. Several sulfur granules within the cell are also visible.

Movie S1

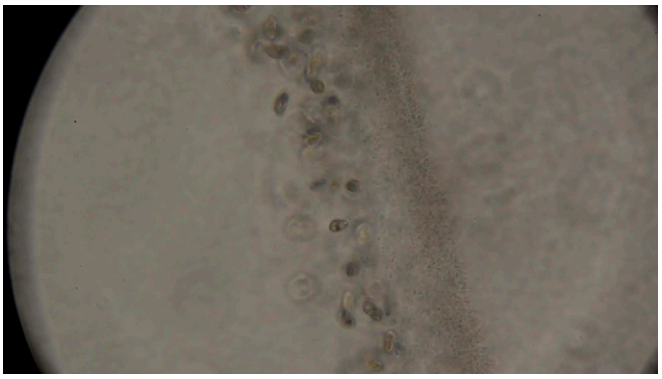

**Movie S2.** Veil.avi (Fig. 1*B* of the main text). Cells are seen attached to the a veil composed of many intertwined tethers. Although most cells swim attached to the veil, a fraction of cells are free swimming. Over the course of the movie, the tethers of several attached cells break, causing them to detach from the veil. Several other cells attach to the veil. Cells are oriented toward oxygen-rich medium.

Movie S2

**Movie S3.** Veil_timelapse.avi. To view the formation of a veil within a front of cells it is easier to perturb an existing veil than to observe the formation of a new front. We perturb the veil chemically. We begin with a front of cells that has already formed a veil. By tilting the chamber slightly, we mix the oxygen around the veil. Cells detach from the veil and form a new front where the oxygen concentration $c = c^* = 4\%$ atmospheric concentration. Over the course of hours, cells within the front aggregate and form a veil. Shown is 7.3 h of the formation of a veil in a front of cells. The width of the frame is 5 mm. Cells appear as bright yellow ovals. The veil material is white.

Movie S3

**Movie S4.** Front_1.avi. Fronts propagating up an oxygen gradient. A photograph of this experiment is shown in Fig. S2. To improve the image quality, we average all of the images in a given experiment and subtract the average image from each frame. As the front is the only object moving in these experiments, it is made clearly visible. Each movie is sped up by a factor of 4,500×. In each case, the front forms at the base of the test tube. As it moves up the gradient, it generates millimeter-scale dimples that attract one another. The mechanism by which these dimples form is discussed in the main text. When the front reaches the surface, it collapses back onto itself. As it falls down the tube it peals veil material from the walls. This material may be formed by cells of density $n_0$ in the tail of the front.

Movie S4

**Movie S5.** Front_2.avi. Fronts propagating up an oxygen gradient. A photograph of this experiment is shown in Fig. S2. To improve the image quality, we average all of the images in a given experiment and subtract the average image from each frame. As the front is the only object moving in these experiments, it is made clearly visible. Each movie is sped up by a factor of 4,500×. In each case, the front forms at the base of the test tube. As it moves up the gradient, it generates millimeter-scale dimples that attract one another. The mechanism by which these dimples form is discussed in the main text. When the front reaches the surface, it collapses back onto itself. As it falls down the tube it peals veil material from the walls. This material may be formed by cells of density $n_0$ in the tail of the front.

Movie S5

**Movie S6.** Front_3.avi. Fronts propagating up an oxygen gradient. A photograph of this experiment is shown in Fig. S2. To improve the image quality, we average all of the images in a given experiment and subtract the average image from each frame. As the front is the only object moving in these experiments, it is made clearly visible. Each movie is sped up by a factor of 4,500×. In each case, the front forms at the base of the test tube. As it moves up the gradient, it generates millimeter-scale dimples that attract one another. The mechanism by which these dimples form is discussed in the main text. When the front reaches the surface, it collapses back onto itself. As it falls down the tube it peals veil material from the walls. This material may be formed by cells of density $n_0$ in the tail of the front. Often, as here, several fronts form in succession. In this movie, a propagating front is annihilated as veil material from the previous front peals from the wall. The front reforms from the cloud of dispersed material and continues up the gradient.

Movie S6

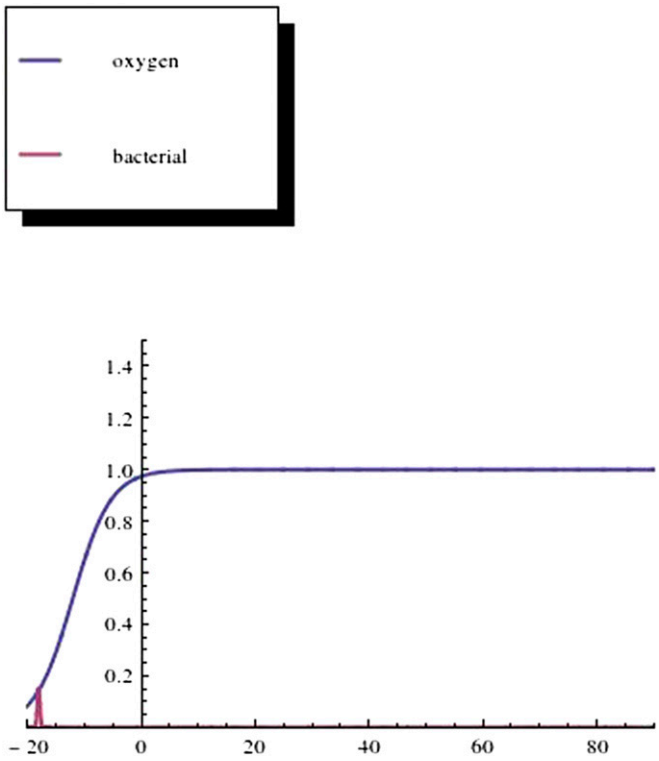


**Movie S7.** 1d_veil.avi. Here we show the time evolution of an initial distribution of cells in an oxygen gradient. We numerically integrate Eqs. **4** and **5** from the main text. It is shown that, after a brief transient, the initial conditions converge to the translating solution. The cell density of the bacterial swarm is shown in red. The oxygen concentration is shown in blue. The formation of a propagating front is a generic feature of these equations for a large range of parameters. In this simulation, we have chosen parameters to accentuate the leading edge of the front so that the tail of the front can be clearly seen. We chose $c^* = 0.5$, $B_0 = 1$, $R_0 = 1$, $\chi'(c) = 10^2$, and $D_n = D_c = 1$.

Movie S7

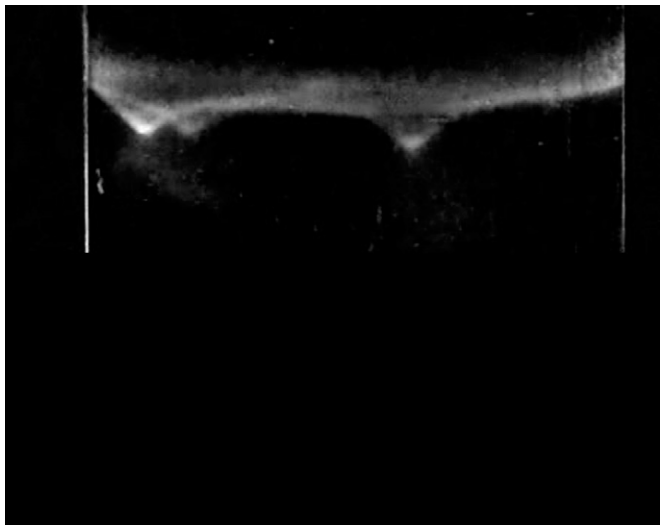

**Movie S8.** Dimples.avi. To observe the formation and evolution of dimples, it is useful to move to the reference frame of the front. Movies S8–S11 show dimples forming in fronts. In "dimples.avi", dimples form continuously and attract one another. When a dimple forms or two join, the opaque wake behind it momentarily intensifies.

Movie S8

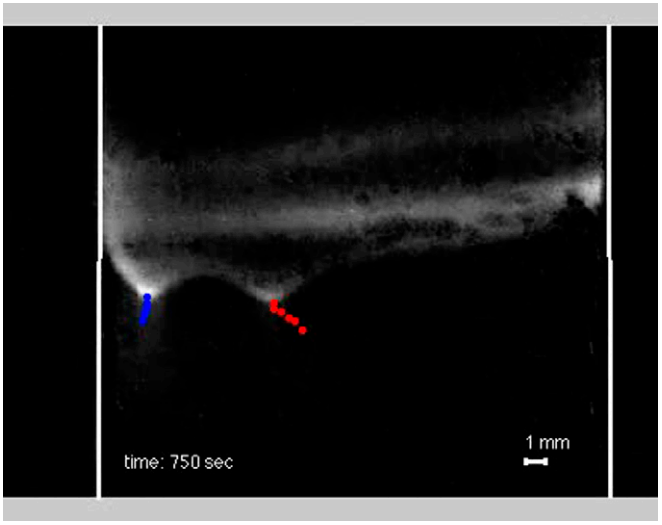


**Movie S9.** veil_star.avi. In these movies, two dimples are shown moving together and joining. In Fig. 4 of the main text, we show the relationship between the distance separating the dimples and their velocity toward one another. The names of the movies correspond to the symbols used in Fig. 8.

Movie S9

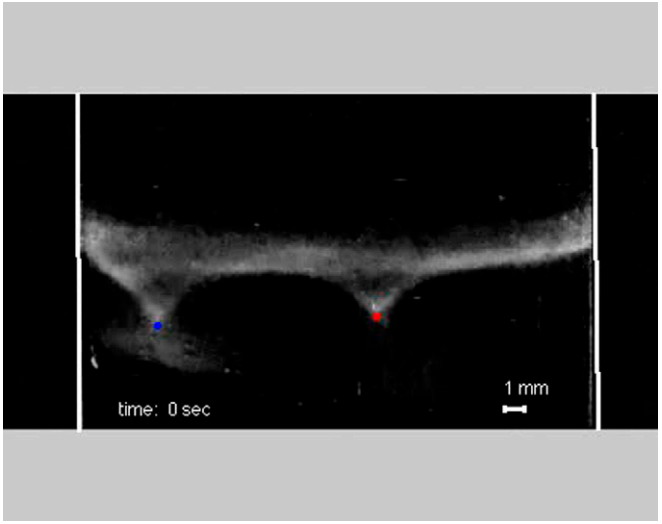


**Movie S10.** veil_triangle.avi. In these movies, two dimples are shown moving together and joining. In Fig. 4 of the main text, we show the relationship between the distance separating the dimples and their velocity toward one another. The names of the movies correspond to the symbols used in Fig. 8.

Movie S10

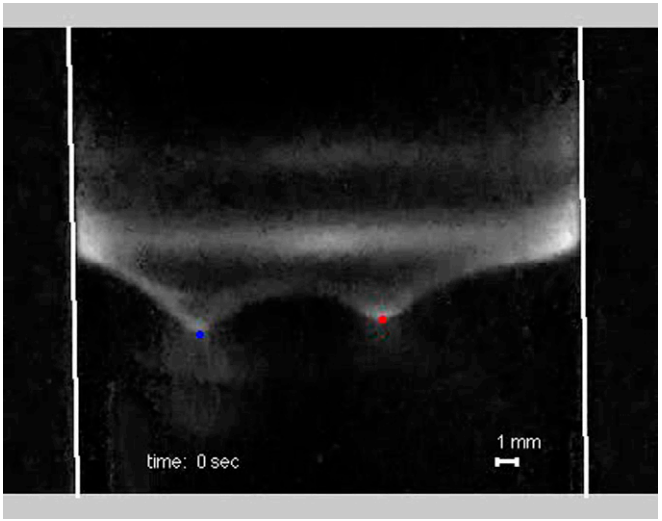


**Movie S11.** veil_circle.avi. In these movies, two dimples are shown moving together and joining. In Fig. 4 of the main text, we show the relationship between the distance separating the dimples and their velocity toward one another. The names of the movies correspond to the symbols used in Fig. 8.

Movie S11